Journal of Materials Chemistry B

Plasmonic Gel Nanocomposites for Detection of High Energy Electrons

Journal:	*Journal of Materials Chemistry B*
Manuscript ID	TB-ART-01-2020-000241
Article Type:	Paper
Date Submitted by the Author:	28-Jan-2020
Complete List of Authors:	Subramaniam, Karthik; Arizona State University, Chemical Engineering Inamdar, Sahil; Arizona State University, Chemical Engineering Dutta, Subhadeep; Arizona State University, School of Molecular Sciences Bista, Tomasz; Banner MD Anderson Cancer Center Sokolowski, Thaddeus; Banner MD Anderson Cancer Center Sapareto, Stephen; Banner MD Anderson Cancer Center Rege, Kaushal; Arizona State University, Chemical Engineering

Plasmonic Gel Nanocomposites for Detection of High Energy Electrons

Karthik Pushpavanam[1#], Sahil Inamdar[1#], Subhadeep Dutta[2#], Tomasz Bista[3], Thaddeus Sokolowski[3], Stephen Sapareto[3] and Kaushal Rege[1(*)]

[1]Chemical Engineering, Arizona State University, Tempe, AZ, 85287

[2]School of Molecular Sciences, Arizona State University, Tempe, AZ, 85287

[3]Banner-MD Anderson Cancer Center, Gilbert, AZ, 85234

[(*)]Corresponding Author
Kaushal Rege, Ph.D.
Chemical Engineering
501 E. Tyler Mall, ECG 303
Arizona State University
Tempe, AZ 85287-6106
Email: rege@asu.edu
Phone: 480-727-8616
Fax: 480-727-9321

# - Equal contribution

ABSTRACT

Radiation therapy is a common treatment modality employed in the treatment of cancer. High energy photons have been the primary source of radiation but when administered, leave an exit dose resulting in radiation damage to the adjacent healthy tissues. To overcome this, high energy electrons are employed in cases of skin cancer to minimize radiation induced toxicity. Despite these advances, measurement of delivered radiation remains a challenge due to limitations with existing dosimeters including labor intensive fabrication, complex read-out techniques and post-irradiation instability. To overcome these limitations, we have developed a novel colorimetric plasmonic gel nanocomposite for the detection of therapeutic levels of radiation delivered in electron beam therapy. The plasmonic nanocomposites consists of an agarose gel matrix encapsulating precursor gold ions which are reduced to gold nanoparticles as a result of exposure to high energy electrons. The formation of gold nanoparticles renders a change in color to the agarose matrix, resulting in the formation of plasmonic gel nanocomposites. The intensity of the color formed exhibits a linear relation with the delivered electron dose, which can be quantified using absorbance spectroscopy. The plasmonic gel nanocomposites were able to detect doses employed in fractionated electron therapy, including in an anthropomorphic phantoms used for planning radiation treatments in the clinic. Furthermore, the use of glutathione as a quenching agent facilitated qualitative and quantitative spatial mapping of the delivered dose. Our results indicate that the ease of fabrication, simplicity of detection and quantification using absorbance spectroscopy, determination of spatial dose profiles, and relatively low costs, make the plasmonic gel nanocomposite technology attractive for detecting electron doses in the clinic.

INTRODUCTION

Radiotherapy, including high energy photons (e.g. X-rays) is commonly used in the treatment of cancer.[1, 2] However, when photons are delivered to a tumor site a large amount of exit dose outside the target volume results in radiation-induced toxicity.[3, 4] To overcome this, high energy charged particles (electrons) are employed in clinical radiotherapy (e.g. Skin cancer)[5]. The physical characteristics of electrons result in a high surface dose and are often used to treat superficial lesions.[6] Electron beams have an inherent property of depositing their maximum dose at the required depth beyond which there is a sharp fall-off.[7] This radiation dose fall-off result in sparing of healthy tissue from undesirable damage and warrants the use of electron beam radiotherapy over high energy photons especially for skin malignancies.[8] Characteristics such as uniform dose deposition, altering dose depth by mere change in beam energy and ease in treatment planning make ionizing electrons a viable option for treatment of cancerous lesions.

Rapid advancements in radiation delivery have led to the use of higher radiation doses resulting in shorter treatment times with similar cure rates.[9, 10] However to ensure patient safety and treatment efficacy during treatment, accurate measurement of the delivered dose is critical. Conventionally used dosimeters include thermoluminescent dosimeters (TLDs), radiochromic films and semiconductor diodes have significant drawbacks. Measurements using TLDs can be time consuming and labor intensive, which makes their routine operation cumbersome[11]. Semiconductor diodes with their accurate readout are limited due to its dose rate dependence which limits their frequent operation.[12] Radiochromic films lack the ability to conform and adapt onto patient specific anatomy, which makes them prone to positional instability and dose inconsistency

with the delivered and predicted dose.[13, 14] In addition, the long times required for developing the color is also a limitation. Thus, there is a need for new technologies that can detect doses in the therapeutic window while addressing all the above challenges.

Recent advancements in molecular, nanoscale and nanocomposite systems can lead to new tools for the detection of therapeutic levels of ionizing radiation.[15] A silver nanoparticle dispersion encapsulated in a sucrose acetate isobutyrate matrix was employed as a sensitive dosimeter to detect therapeutic levels of ionizing radiation. However, this system relied on positron emission tomography (PET) for quantification potentially hindering clinical translation due to the requirement of a sophisticated equipment.[16] A single-walled carbon nanotube – poly(olefin sulfone) nanocomposite which underwent depolymerization under ionizing radiation was investigated for radiation detection.[17] Although the system facilitated real-time detection of ionizing radiation, the dosimeter will need to be further optimized to detect therapeutic levels of radiation.[17] Quantum dot nanoparticles dispersed in polyvinyltoluene demonstrated excellent scintillating properties under ionizing radiation but were unable to spatially resolve regions only exposed to ionizing radiation[18]. Despite these advances and their concomitant limitations, there is a need to develop novel technologies that require minimal chemical processing and facilitate a simple, quantifiable read-out for the detection of ionizing electrons used in clinical radiotherapy.

Gold nanoparticles possess unique optical and physiochemical properties and have found application in diagnostics, imaging and drug delivery.[15, 19-22] Taking advantage of the plasmonic properties of gold nanoparticles, we designed different formulations of colorimetric liquid sensors which, upon exposure to ionizing radiation (photons), resulted in the formation of gold

nanoparticles from its colorless precursor salt solution.[23-25] The sensor was further modified to facilitate easy handling and alleviate application concerns through formulation of the precursor salt solution in a hydrogel matrix, resulting in the generation of plasmonic nanocomposites upon exposure to ionizing radiation as an indicator of ionizing radiation.[26-28]

In this study, we describe generation of gold nanoparticles within a hydrogel in response to different doses of therapeutic ionizing electrons as a novel detection system. Formation of gold nanoparticles results in a visible color change (e.g. maroon) of the nanocomposite from an initially colorless hydrogel. The intensity of color increases with increasing amount of radiation and is used to quantify the delivered dose. Finally, the ability of the plasmonic nanocomposites to capture topographical dose profiles using a fixing agent post irradiation is reported. To the best of our knowledge, the generation of plasmonic nanocomposites for electron beam dosimetry is the first of its kind and has high potential for translation to clinical applications.

Materials and Methods

Materials. Molecular biology grade agarose, L-ascorbic acid (AA), dodoceyltrimethylammonium bromide (C_{12}TAB; ≥98%), Glutathione reduced (≥98%), gold(III) chloride trihydrate ($HAuCl_4.3H_2O$) and myristyltrimethylammonium bromide (C_{14}TAB; ≥99%) were acquired from Sigma-Aldrich. Cetyltrimethylammonium bromide (C_{16}TAB) was obtained from MP Chemicals. Sodium dodecylsulfate (SDS) was obtained from Bio-Rad Laboratories and Tween 20 was purchased from Fisher Scientific. All chemicals were employed in the study without further

processing or purification. The solvent employed in the study was MilliQ water (Resistivity: 18.2 MΩ.cm).

Generation of Plasmonic Gel Nanocomposites following Irradiation with Ionizing Electrons. A 24 well plate was used as a mold in order to fabricate hydrogel disks with diameters of ~1.5 cm and thickness of 3 mm. Briefly, 600 µL of a 50 mM stock solution of C_xTAB (x = 12, 14, 16) was prepared and mixed with 30 µL of 10 mM $HAuCl_4$ in 1.7 mL microcentrifuge tubes. From this mixture, 100 µL was removed prior to the addition of heated 2% liquid agarose (500 µL). From this mixture, 650 µL was removed and poured into the molds of the well plate and allowed to set as gels prior to irradiation experiments. The gels were then incubated in 10 mM ascorbic acid (650µL) for 10 minutes resulting in translucent hydrogels. The final concentration of $HAuCl_4$, C_xTAB and agarose were 0.25 mM, 25 mM, and 1% (w/v) respectively.

A 6 well plate was used as a mold for fabricating larger hydrogel disks with diameters of ~3.5 cm and thickness of 3 mm. Briefly, 1.63mL of a 75 mM stock solution of $C_{14}TAB$ was prepared and mixed with 81.6 µL of 10 mM $HAuCl_4$ in a 15 mL microcentrifuge tubes. From this mixture, 272 µL was removed prior to the addition of heated 2% liquid agarose (1.44 mL). This mixture (2.88 mL) was poured into well plates and allowed to set as gels prior to electron irradiation experiments. The gels were then incubated in 10 mM ascorbic acid (2.88 ml) for 10 minutes resulting in translucent hydrogels. The final concentrations of $HAuCl_4$, $C_{14}TAB$ and agarose were 0.25 mM, 37 mM, and 1% (w/v) respectively.

Electron beam Irradiation. All experiments were conducted at the Banner-MD Anderson Cancer Center in Gilbert, AZ using a Varian Truebeam linear accelerator radiation therapy system. The energy and dose rate of the beam were set at 6 MeV and 600 MU/min unless otherwise mentioned. A standard field size of 10 cm x 10 cm was maintained throughout the study. For spatial dose deposition, only half the gel was placed in the irradiation field. Post irradiation, further analyses was carried out at Arizona State University in Tempe, AZ (approximate travel time of 30 minutes).

Post-processing of Plasmonic Nanocomposites. Glutathione, a naturally occurring antioxidant (reductant) was used as a post processing agent in order to quench the formation of gold nanoparticles within agarose gels. Glutathione (25mM) was added from the top of the gel, 30 minutes post electron irradiation and the gel was incubated for 10 minutes. The volumes used for incubation were 650 μL for gel nanocomposites with diameters of 1.5 cm and ~2.9 mL for gel nanocomposites with diameters of 3.5 cm, respectively. The residual glutathione from the surface of the plasmonic gel nanocomposites was discarded. Furthermore, the absorbance of the gels was determined for quantification electron dose.

Absorbance Spectroscopy. Absorbance spectra for all samples were obtained using a BioTek Synergy™ 2 plate reader. Absorbance values were measured from 300 nm to 990 nm with a step size of 10 nm; MilliQ water was used as blank for all spectroscopy experiments. Absorbance values at 990nm were subtracted from the absorbance values at all wavelengths in order to normalize the absorbance spectra for further analyses. Although the change in color was observable 15 minutes post irradiation, absorbance measurements were carried out two hours post irradiation because of travel time between Banner M.D Anderson Cancer Center in Gilbert, AZ and Arizona State

University in Tempe, AZ (approx. travel time 30 min). Absorbance values at a wavelength of 540 nm, which is typically the peak absorption wavelength for gold nanoparticles, were plotted as a function of electron radiation dose in order to generate a calibration curve. The efficacy of gel nanocomposite was evaluated by predicting for unknown test doses using the calibration curve and which is used to determine unknown radiation doses.

Topographical Mapping of Plasmonic Nanocomposites. A 1536 well plate set up, with a grid size of ≈2mm x 2mm, in a BioTek Synergy™ 2 plate reader was employed to map the topographical distribution of electron doses. Absorbance values at 540 nm and 990 nm were measured at each individual grid along the entire gel surface, leading to a pixelated dose map of the gel surface. The final absorbance was calculated by subtracting the absorbance values of water and 990 nm wavelength from the absorbance value at 540 nm wavelength. The calibration curve was used to predict the delivered dose to each cell of the grid corresponding to its topographical dose map over the gel surface.

Transmission Electron Microscopy (TEM). Following electron irradiation, the plasmonic gel nanocomposites were dissolved in 1,2-propanediol, a chaotropic agent, to facilitate removal of excess agarose by gently heating at 80°C for 15 min.[29] The resultaing liquefied hot mixture was centrifuged at 4000 rpm for 10 mins and the supernatant, i.e. agarose-propane diol mixture, was discarded carefully to isolate the pellet containing gold nanoparticles. The pellet was further dispersed in deionized water. From this, gold nanoparticle samples for TEM imaging were prepared by casting a drop of the resuspended pellet onto a carbon film placed on a TEM grid. The samples were dried overnight in air. A CM200-FEG instrument operating at 200 kV in the LeRoy

Eyring Center for Solid State Sciences at ASU was used for imaging of gold nanoparticles formed in the gels following irradiation with ionizing electrons.

Detection of Electron Dose in an Anthropomorphic Thorax Phantom using Plasmonic Gel Nanocomposites. An anthropomorphic thorax phantom was positioned on a radiotherapy table and aligned using guiding lasers as described in previous studies.[30] The gel formulation was positioned in the middle of a 10 cm x 10 cm radiation field in order to quantitatively detect the delivered dose. A 1.3 cm tissue-equivalent bolus was placed on top of the plasmonic nanocomposites in order to attain charge equilibrium near the surface of the anthropomorphic phantom. The phantom was irradiated with an electron dose of 2.5 Gy following which the gel was retrieved and evaluated for absorbance and associated electron dose as described in the previous sections.

Image Acquisition. All images were acquired using a HPLaserJet 3390 scanner or an Apple iPhone 7. Furthermore, images were cropped to the required size and no further editing or post processing of the images was carried out.

Statistical Analyses. All experiments were performed in quintuples unless otherwise specified. Data analyses for all independent experiments were performed using Microsoft Excel. Data reported in the manuscript are represented as mean ± one standard deviation.

Results and Discussion

Electron beam therapy is frequently used for the treatment of superficial layers (epidermis and dermis) of malignant skin lesions[31]. Fractionated electron beam therapy involves delivering a cumulative dose of 20-70 Gy in fractions of 1-2 Gy per session over a course of several weeks[32]. There is a need to ensure precise and accurate delivery of electron radiation to patients in order to avoid overexposure, which can lead to physiological complications. Whole body exposure to 1 Gy radiation results in gastrointestinal and neurovascular symptoms while focused 3 Gy skin dose are likely to result in skin burns.[33] Current devices used for dosimetry are complex to fabricate and cumbersome to operate, which limits their routine clinical use. Thus, there is still a critical need for the development of facile radiation detection devices that are robust, easy to fabricate and operate, which will lead to improved patient safety during radiotherapy.

The principle behind radiation-induced generation of plasmonic gel nanocomposites is the reduction of trivalent gold ions to monovalent gold ions and then to gold nanoparticles following reduction by free radicals generated upon exposure to high energy electrons. It is thermodynamically more favorable to reduce gold present in its monovalent state Au(I) to the zerovalent state compared to the reduction of trivalent Au(III) to the monovalent state. However, gold present in $HAuCl_4$, is in the trivalent state[34] and thus, a room temperature reduction reaction was carried out using ascorbic acid (Vitamin C) in order to bring the gold to a monovalent state.

High energy electrons employed in the study for irradiation can likely participate in both direct as well as indirect (i.e. radiolysis-based) mechanisms of reduction of Au(I) to Au(0). Exposure to ionizing radiation involves generation of reactive free radicals including hydrated electrons (e^-_{aq}),

hydrogen free radicals ($H^{\cdot}$) and hydroxyl free radicals ($OH^{\cdot}$) through the splitting of water (radiolysis)[35]. Hydrated electrons (e^{-}_{aq}) and hydrogen free radicals ($H^{\cdot}$) promote reduction of monovalent Au(I) ions to zerovalent Au(0) ions. Although $OH^{\cdot}$ is an oxidizing agent and can impede nanoparticle formation through dissolution of Au(0), the presence of ascorbic acid (anti-oxidant) potentially minimizes these unfavorable side reactions[36].

Reduction of trivalent gold ions to monovalent gold ions was carried out in the presence of three distinct surfactants, i.e. cationic, anionic and non-ionic surfactants, to investigate the stability of the monovalent gold ions. Addition of ascorbic acid in presence of sodium dodecylsulfate (anionic) and Tween-20 (non-ionic surfactant), resulted in the development of a pink/purple color and a characteristic peak between 500 nm and 600 nm in the UV-visible region of the absorption spectrum suggesting spontaneous formation of gold nanoparticles (**Figure 1**). However, in presence of the cationic surfactant, a color change was not seen and no characteristic peak was seen in the UV-visible region of the light absorption spectrum, which suggests the lack of spontaneous gold nanoparticle formation (**Figure 1**). The formation of this colorless solution is indicative of formation and persistence of Au(I) ions in the mixtrure[37]. We hypothesize that the favorable electrostatic interaction between the negatively charged tetrachloroaurate ions and positively charged cationic surfactant molecules leads to enhanced shielding of Au(III) to ascorbic acid thereby inhibiting spontaneous gold nanoparticle formation. Based on these observations, we employed cationic surfactants for our subsequent irradiation studies.

In order to further facilitate easy handling and mitigate concerns during clinical translation, the molecular components that make the detection system, namely gold salt, cationic surfactant and

ascorbic acid, were loaded in an agarose hydrogel matrix. Agarose gel formulations have received attention as controlled drug release platforms and as scaffolds for regenerative tissues due to their low toxicity[38]. Agarose was chosen as the hydrogel matrix for our plasmonic gel nanocomposite sensor based on its biocompatibility, ease in modulation of mechanical properties, and simplicity in fabrication of the hydrogel[38].

Plasmonic gel nanocomposites with diameters ≈ 1.5cm and thicknesses ≈ 3mm were fabricated with three different cationic surfactants (C_xTAB) with varying chain lengths (x = 12, 14 and 16) and their response to therapeutic levels of high-energy electrons irradiation (0-5 Gy) were determined. In all cases, exposure to high energy electrons (0-5 Gy) rendered a maroon color to the hydrogel due to the formation of gold nanoparticles while the non-irradiated control remained colorless (**Figure 2**). Exposure of the detection gels to increasing levels of high energy electrons resulted in a direct increase in the number of reducing species, which, in turn, led to a higher probability of reduction of Au(I) to Au(0) ions. Further nucleation and growth of Au(0) results in the formation of gold nanoparticles imparting the characteristic color (maroon) to the hydrogel. This was manifested as an increase in the intensity of color.

The change in color from colorless to maroon for C_{12}TAB-, C_{14}TAB- and C_{16}TAB-loaded, hydrogels was observed ~5, ~10, and ~15 minutes post irradiation, which indicates that varying the chain length of the surfactant affects the sensitivity of the plasmonic nanocomposites to high energy electrons. Specifically, for a fixed radiation dose of 3 Gy decreasing the chain length of the cationic surfactant resulted in an increase in absorbance from 0.01 to 0.13 in the developed color in the plasmonic gel nanocomposite. The color formation in the plasmonic gel nanocomposites

was further quantified using absorbance spectroscopy two-hour post irradiation (**Figure 3**). A characteristic spectral peak between 500 and 600 nm, with a peak absorbance at 540 nm, indicative of gold nanoparticle formation[39] in the gel, was used to quantify the color formed. The absorbance at 540nm increased with increasing dose of high-energy electrons, which corroborates the observed increase in color intensity (**Figure 3D**).

At the concentrations employed in the study (final concentration ≈25 mM), all cationic surfactants employed in the study form micelles.[40] Gold nanoparticle growth is governed by the frequency of collisions between $AuBr_2^-$ bound cationic micelles and with zerovalent Au(0) ions generated following radiolysis by high-energy electrons; nanoparticles formed in the gel are stabilized by the cationic surfactant in the plasmonic nanocomposites.[41, 42] We hypothesize that decreasing chain length results in increasing diffusion coefficients of the micelles.[43] This increased mobility could potentially result in an increased frequency of collisions between $AuBr_2^-$ bound cationic micelles and radiation-generated Au(0) ions, which results in higher yields of gold nanoparticles with decreasing order of cationic chain length. Transmission electron microscopy **(Figure 4**) illustrates a relatively non-homogenous distribution of gold nanoparticle sizes and shapes formed upon irradiaton with high-energy electrons; an average particle size ≈ 54 ± 17nm was seen upon irradiation with a 4 Gy dose. Although C_{12}TAB- and C_{16}TAB-containing hydrogels were also capable of nanoparticle formation, C_{14}TAB was employed for all further experiments due to its linear response between 0 and 5 Gy.

Clinical radiotherapy involves radiation field sizes larger than 1 cm^2.[44] Consequently, we fabricated larger gel detectors (≈ 3.5 cm diameter and ≈ 3 mm thickness) in order to adopt the

detection technology to larger field sizes. Topographical detection of irradiated electron doses can facilitate mapping over large surface areas of tissues including skin. We therefore irradiated one half of the gel detector with an electron dose of 3Gy. A change in color was indeed observed only in that half, but a "bleed-over" of color to non-irradiated regions was observed over a period of time. (**Figure 5A**); this leads to a loss in topographical information of the dose. This is likely because radiation-generated gold nanoparticles in the irradiated regions act as seeds for unreacted $AuBr_2^-$ ions in the non-irradiated regions, facilitating further generation of gold nanoparticles. The formation of further gold nanoparticles, in turn would result in the observed "bleed-over" phenomena leading to a loss in topographical dose information. We recently demonstrated that the use of a quenching agent that arrests the formation of gold nanoparticles helps retain topographical dose information[28]. We reasoned that treatment with glutathione, which is a thiol-containing tripeptide would complex/react with unreacted $AuBr_2^-$ ions and preserve spatial dose information[45]. Incubation with glutathione for 10 minutes (30 minutes post radiation) led to complete arrest of the "bleed-over" phenomena, which allowed the plasmonic gel nanocomposite to accurately report a topographical map of the electron irradiation profile.

The dose at different locations on the gel map were quantified using a calibration curve for absorbance at 540 nm plotted against delivered dose (**Figure 5B and 5C**); the absorbance response saturated beyond 5 Gy. A linear response with a curve-fit equation of $y=0.03x$ (y is the absorbance at 540 nm and x is the dose in Gy) was observed between 0-5 Gy, although the calibration is strictly applicable only between 2-5 Gy. Three unknown pilot doses were employed to verify the efficacy of the plasmonic nanocomposites (**Table 1**). The predictions had very low error for prediction of unknown doses between 2-5 Gy but had a larger error outside this range, as anticipated from the

response seen with the plasmonic gel nanocomposites. These results demonstrate the ability of the electron irradiation induced plasmonic gel nanocomposites to predict delivered doses that are commonly used in fractionated radiotherapy (2-5 Gy).

The ability of the plasmonic nanocomposites for detecting spatial distribution of electrons was evaluated by irradiating half of the plasmonic nanocomposites with 3 Gy (**Figure 6A**). Upon completion of the irradiation, a visual appearance of color was observed in the irradiated region, and the non-irradiated region remains colorless. Glutathione was added 30 minutes post-irradiation in order to preserve the spatial dose profile. The absorbance at 540nm was measured at finite grids of ≈2mm x 2mm along the diameter of the plasmonic gel nanocomposites and these values were used to determine the electronn dose delivered at every location using the calibration in **Figure 5C**. **Figure 6B** shows that the dose predicted from the calibration (predicted) along the diameter of the plasmonic nanocomposites was in agreement with the actual delivered dose. Taken together, these results indicate the potential of the plasmonic gel nanocomposites to qualitatively and quantitatively detect electron doses in clinical radiotherapy.

Radiotherapy involves the use of a wide range of dose rates for the effective treatment of tumors[46]. We next irradiated the gel detectors with different dose rates with a final dose of 3 Gy (**Figure 7**) in order to investigate the effect of dose rates on detection performance. No significant differences were observed in the absorbance response of the different gels, which indicates that the plasmonic gel nanocomposite system is independent to the rate of the electron dose delivered. This may be anticipated because nanoparticle growth is dependent on the final concentration of Au(0) species required for nucleation and growth processes which is independent of rate of reducing species

generation (dose rate) and only dependent on concentration of reducing species (final dose delivered).

We further investigated the efficacy of the gel detector system for predicting electron doses delivered to an anthropomorphic thorax phantom (**Figure 8**). The gel detector system were kept on top of the "skin" of the phantom in the center of the radiation field and irradiated with 2.5 Gy. Absorbance analysis of the plasmonic gel nanocomposite formed indicated a dose of 2.55 ± 0.02 Gy, which is in close agreement to the delivered dose. The percentage error, approximately 2%, is similar to existing dosimeters which have an uncertainty less than 10%.[47] The distinct visual color change, coupled with a simple quantitative measurement (absorbance) indicates the translational potential of this approach for detecting clinically relevant doses of high-energy electrons.

CONCLUSIONS

To our knowledge, this is the first colorimetric plasmonic nanocomposite for the detection and prediction of radiation dose delivered in electron beam radiotherapy. The plasmonic nanocomposites displayed a robust linear calibration between therapeutically relevant radiation dose range (2-5 Gy) using a simple detection method (absorbance spectroscopy). The plasmonic nanocomposites were able to predict the radiation dose administered to anthropomorphic thorax phantoms and demonstrated dose rate independence for detecting clinically relevant doses. We demonstrated the capability of the plasmonic nanocomposites to qualitatively and quantitatively distinguish regions exposed to radiation and not exposed to radiation. The current system possesses several advantages including the simplicity of detection, rapid response (a few minutes) and low

cost. It is likely that the sensitivity and range of this system may be further improved with design of novel catinic surfactants and templating agents. The use of a biocompatible hydrogel can facilitate patient-specific dosimetry depending on the patient anatomy. We anticipate that the plasmonic nanocomposite system has high potential for translation in clinical electron beam therapy.

ACKNOWLEDMENT

This work was funded by a grant from the National Science Foundation (NSF-CBET 1403860) to K.R. We also gratefully acknowledge the use of facilities within the LeRoy Eyring Center for Solid State Science at Arizona State University, Tempe, AZ.

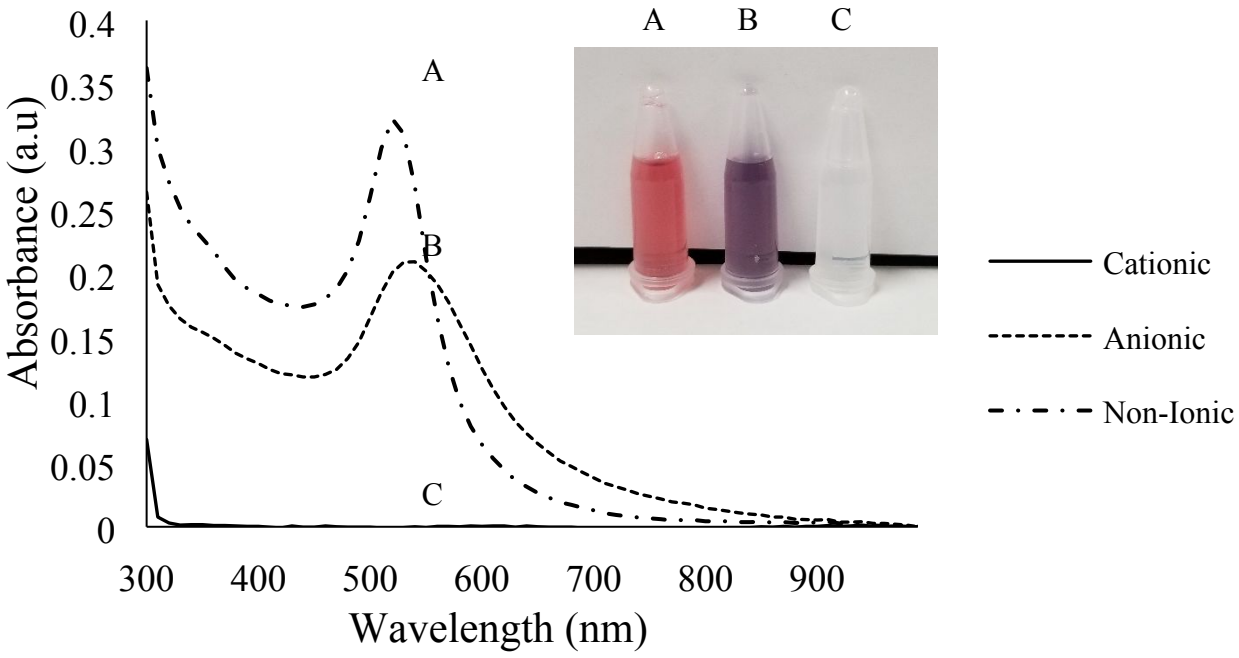

Figure 1. Absorbance spectra and digital images illustrating the presence and absence of spontaneous gold nanoparticle formation with three distinctly charged surfactants. Both anionic and non-ionic surfactants display spontaneous nanoparticle formation in <2 min. as indicated by the presence of a spectral peak between 500-600 nm; no such peak is observed in the presence of cationic surfactant. The inset shows the presence of pink and purple-colored dispersions indicative of formation of gold nanoparticles in presence of anionic and non-ionic surfactants. A colorless solution is seen in case of the cationic surfactant, which indicates absence of gold nanoparticles. The surfactants used are C_{16}TAB (cationic), SDS (anionic) and Tween 20 (non-ionic) at a concentration of 20 mM. The final gold and ascorbic acid concentrations were 0.2 mM and 4 mM respectively. Image Credit: Karthik Pushpavanam, Arizona State University.

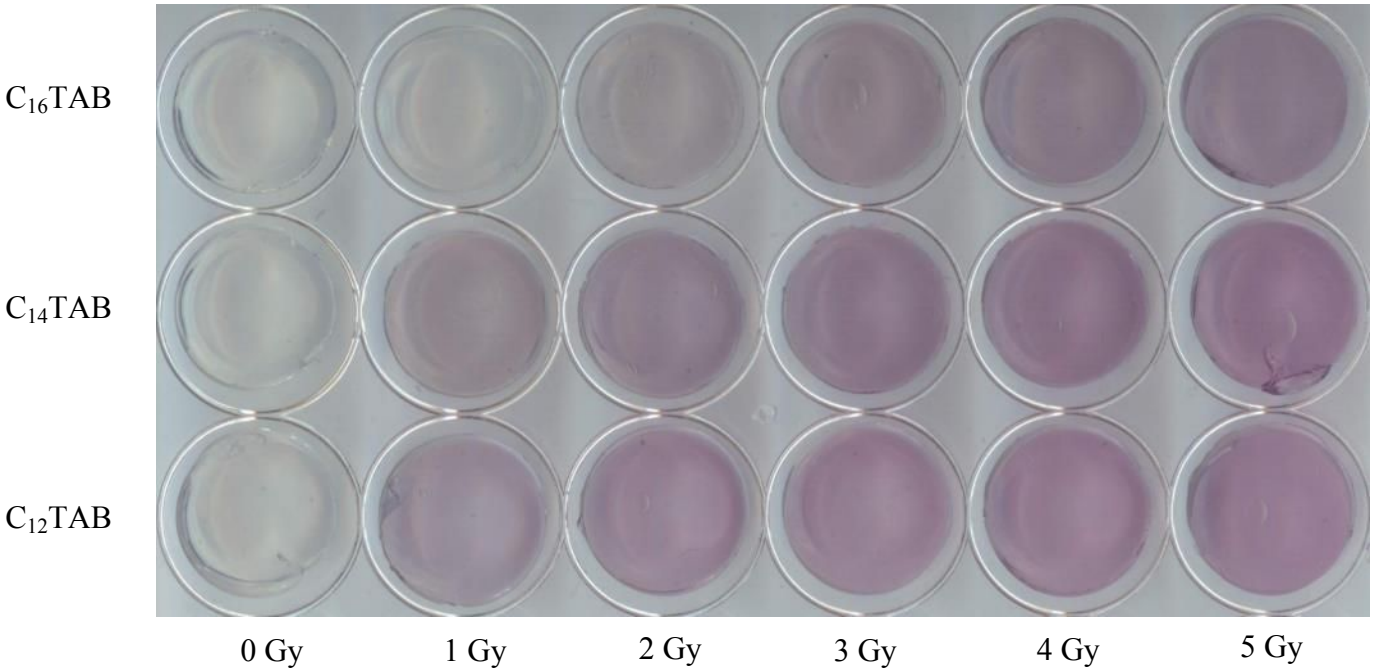

Figure 2. Image of plasmonic gel nanocomposites formed following exposure to different electron doses (Gy) and 25 mM C_{16}TAB (top), C_{14}TAB (middle) and C_{12}TAB (bottom) cationic surfactants. All agarose-based gels contain 0.2 mM $HAuCl_4$, which were subsequently incubated with 10 mM ascorbic acid for 10 mins. All images were taken 2 hours post irradiation with ionizing electrons. glutathione was not added added to the gels post irradiation in this study. Image Credit: Karthik Pushpavanam, Arizona State University.

A

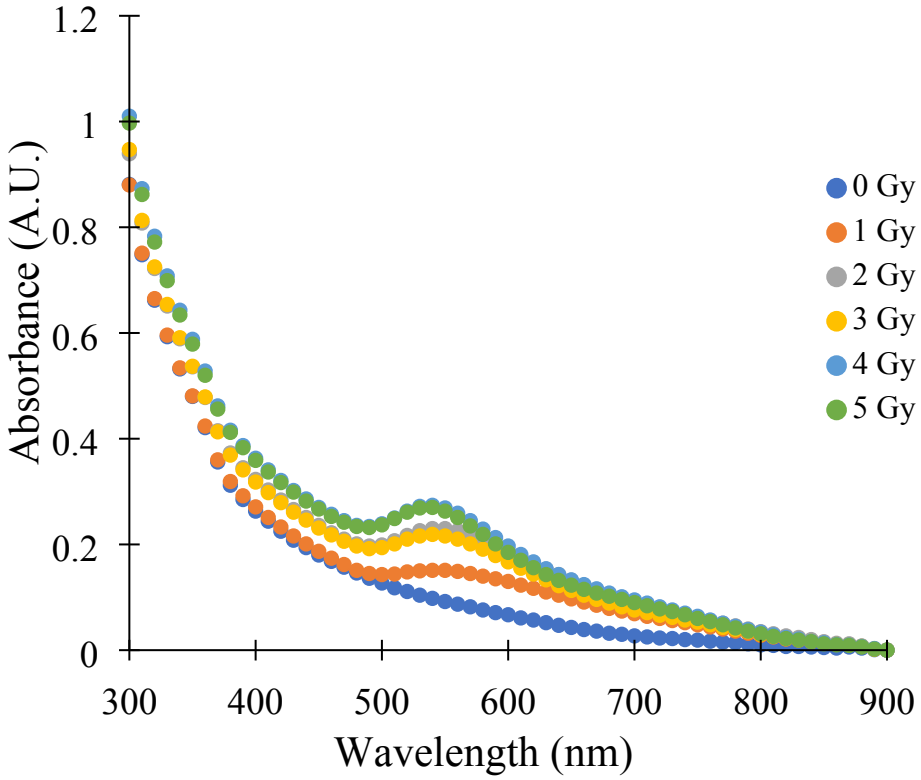
1.2
1
0.8
0.6
0.4
0.2
0
Absorbance (A.U.)
300
400
500
600
700
800
900
Wavelength (nm)
0 Gy
1 Gy
2 Gy
3 Gy
4 Gy
5 Gy

B

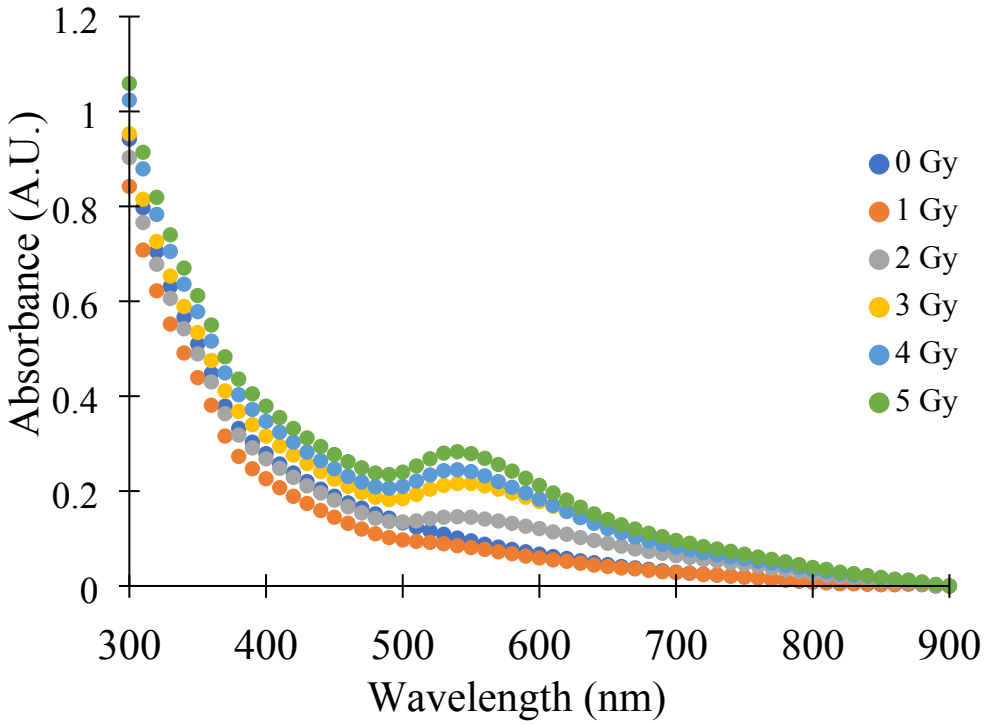
1.2
1
0.8
0.6
0.4
0.2
0
Absorbance (A.U.)
300
400
500
600
700
800
900
Wavelength (nm)
0 Gy
1 Gy
2 Gy
3 Gy
4 Gy
5 Gy

C

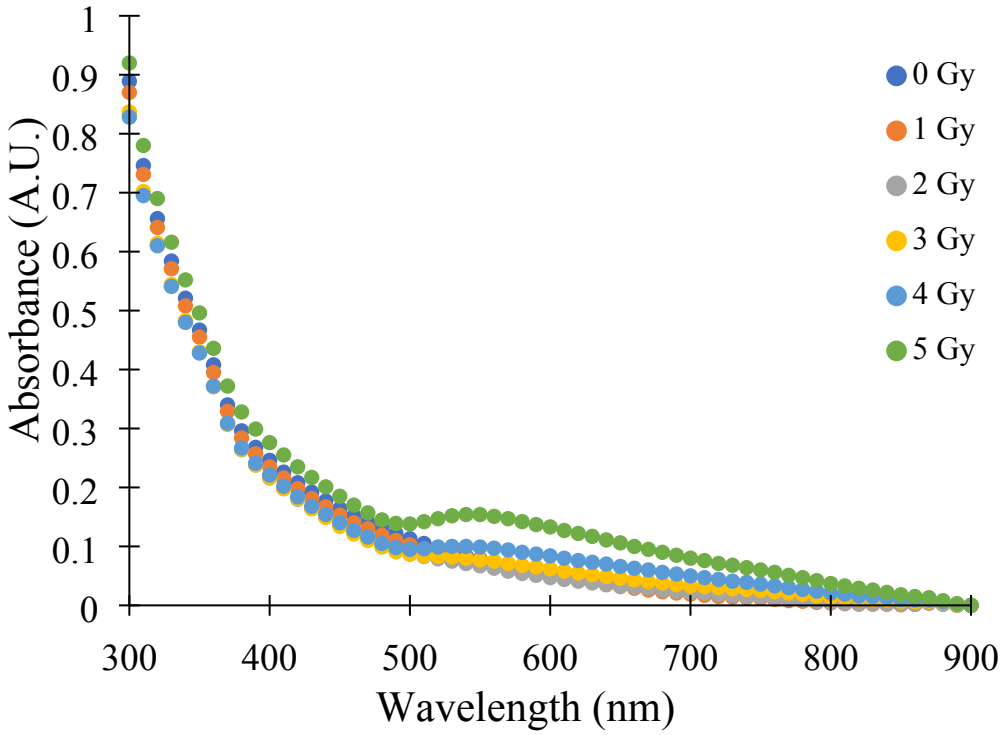
Absorbance (A.U.)
Wavelength (nm)
0 Gy
1 Gy
2 Gy
3 Gy
4 Gy
5 Gy

D

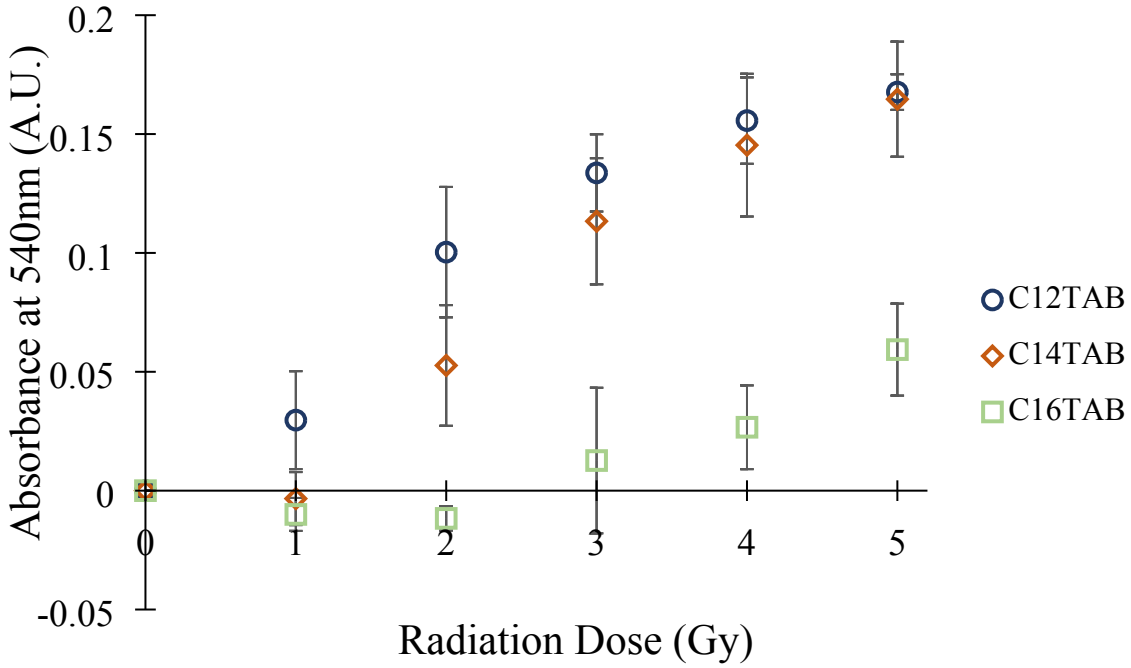
Absorbance at 540nm (A.U.)
Radiation Dose (Gy)
C12TAB
C14TAB
C16TAB

Figure 3. Absorbance spectra of plasmonic nanocomposites following exposure to different doses (Gy) and 25 mM **(A)** C_{12}TAB, **(B)** C_{14}TAB and **(C)** C_{16}TAB cationic surfactants. All agarose-based gels contain 0.2 mM $HAuCl_4$, which were subsequently incubated with 10 mM ascorbic acid for 10 minutes. Appearance of the characteristic peak between 500-600 nm is indicative of gold nanoparticle formation. **(D)** Plot of peak absorbance at 540 nm as a function of radiation dose for C_{12}TAB (blue circles), C_{14}TAB (orange diamonds) and C_{16}TAB (green squares). In all cases, the absorbance of the plasmonic gel nanocomposites were measured 2 hours post irradiation with electrons.

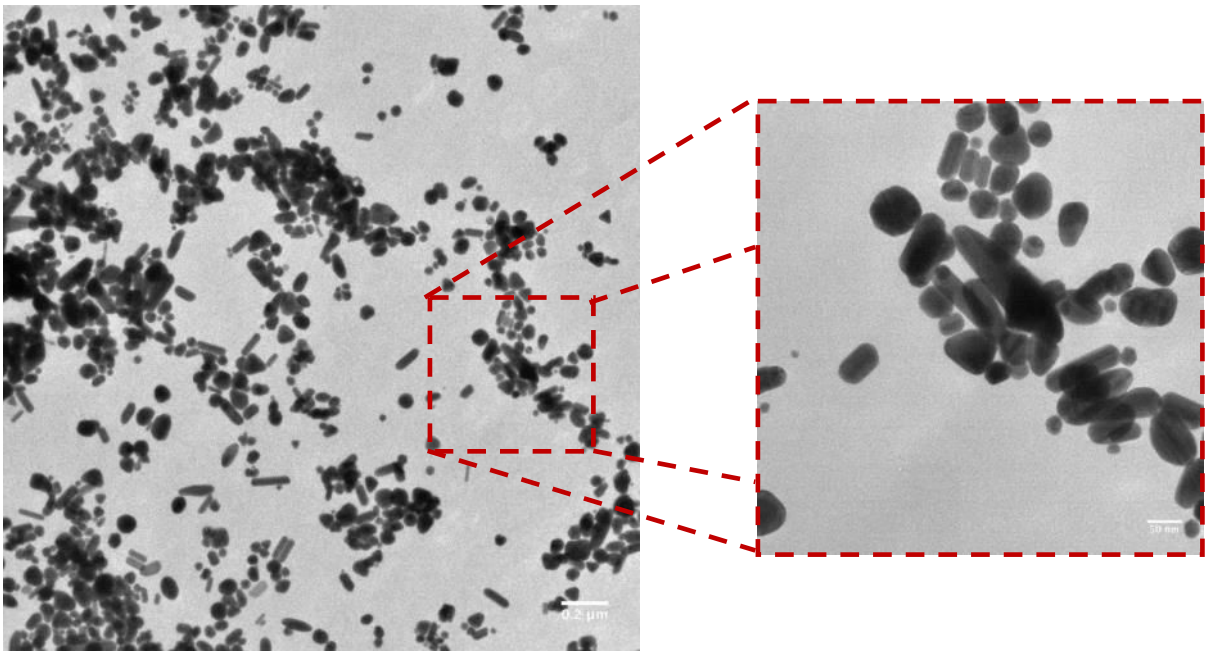

Figure 4. Transmission Electron Microscopy (TEM) micrographs of gold nanoparticles formed with gels containing C_{14}TAB as the cationic surfactant and irradiated with a 4 Gy electron beam dose. (Left) Low magnification image depicting the presence of gold nanoparticles in the dried hydrogel. (Right) High magnification image of the highlighted region (dashed red box). Image Credit: Karthik Pushpavanam, Arizona State University.

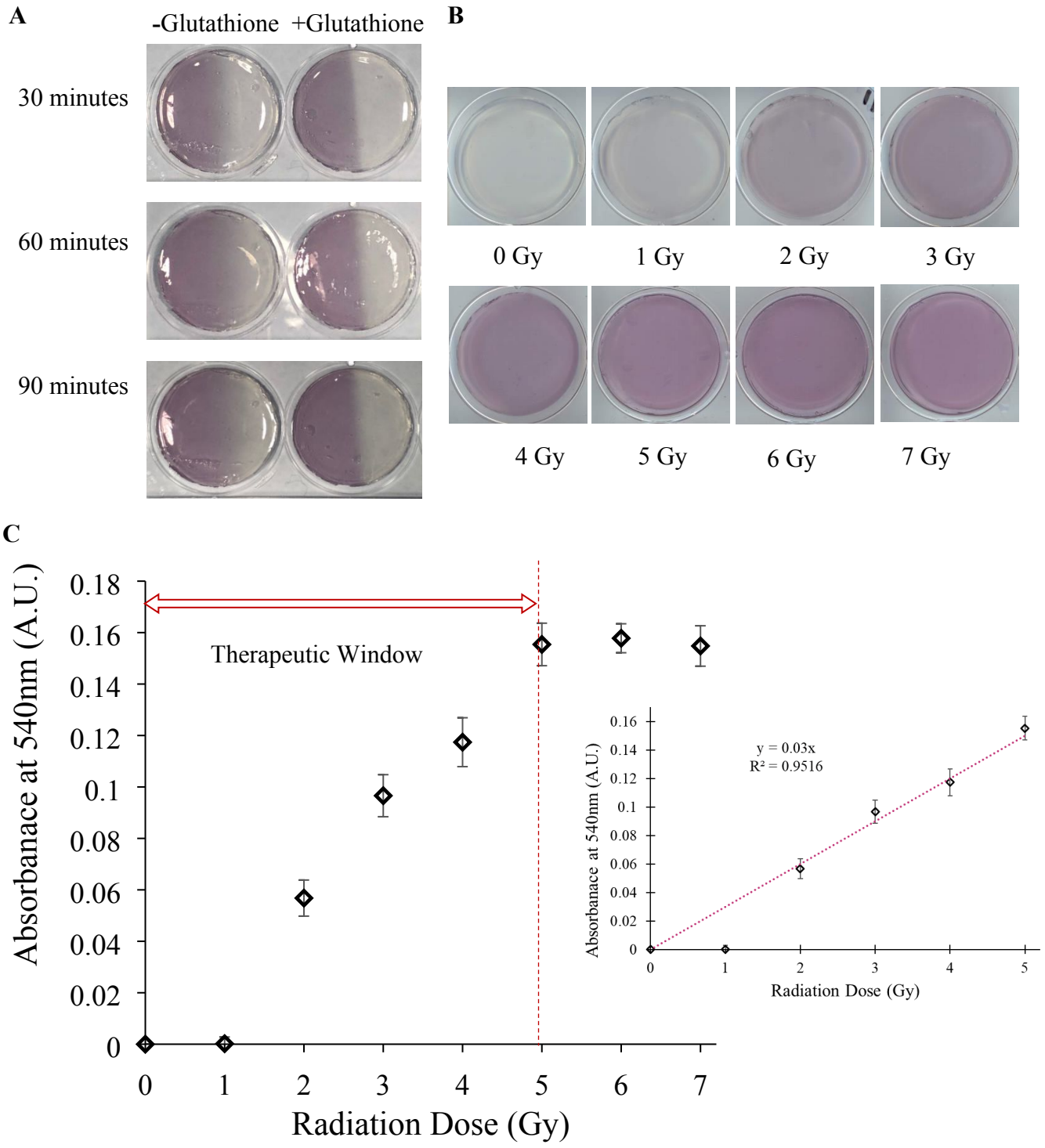

Figure 5. (A) Images of the plasmonic gel nanocomposites irradiated with electrons (3 Gy) and further incubated with (right) or without (left) 25 mM glutathione for 10 minutes; glutathione was added 30 minutes post-irradiation. Topographical dose profile is maintained upon incubation with glutathione. **(B)** Images of plasmonic gel nanocomposites irradiated with different doses of electrons. **(C)** Absorbance of C_{14}TAB-containing plasmonic gel nanocomposites at 540 nm as a

function of radiation dose (0-7 Gy). The linear range in the therapeutic window of the plasmonic gel nanocomposites (2-5 Gy) is indicated. **(Inset)** Calibration curve for C_{14}TAB using absorbance at 540 nm as a function of radiation dose between 0 and 5 Gy. The plasmonic nanocomposites contain 0.2 mM $HAuCl_4$, 37 mM C_{14}TAB, 1% (w/v) agarose and are incubated with 10 mM ascorbic acid for 10 minutes prior to irradiation. At 30 min post irradiation, the plasmonic gel nanocomposites formed were further incubated with glutathione (25 mM) for 10 minutes. All images were taken 2 hours post irradiation. Image Credit for **6A**: Sahil Inamdar, Arizona State University. Image Credit for **6B**: Karthik Pushpavanam, Arizona State University.

A

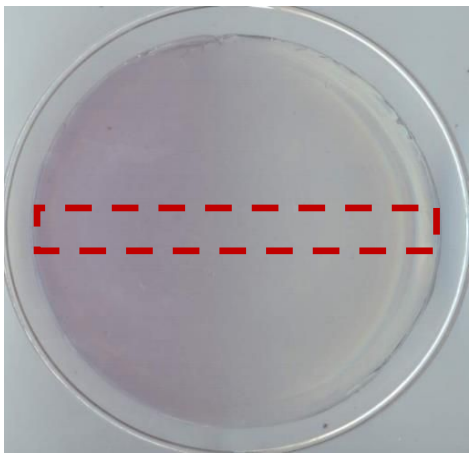

B

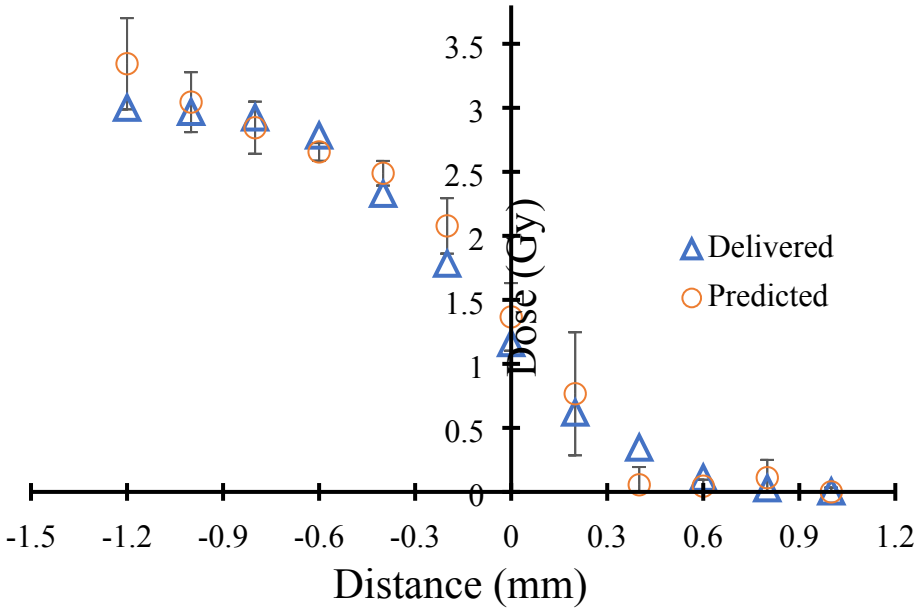

Figure 6. (A) Image depicting the colorimetric response of the plasmonic gel nanocomposites formed in response to a 3 Gy electron dose. The appearance of a maroon color indicates the capability of the plasmonic gel nanocomposites to qualitatively distinguish the irradiated and the non-irradiated regions. **(B)** Dose fall off-profiles comparing the delivered dose (blue triangles) with the predicted dose (orange circles) indicates the efficacy of the plasmonic gel nanocomposites to quantitatively determine the topographical dose profile / map. Please see Experimental section for details on dose quantification. Image Credit: Karthik Pushpavanam, Arizona State University.

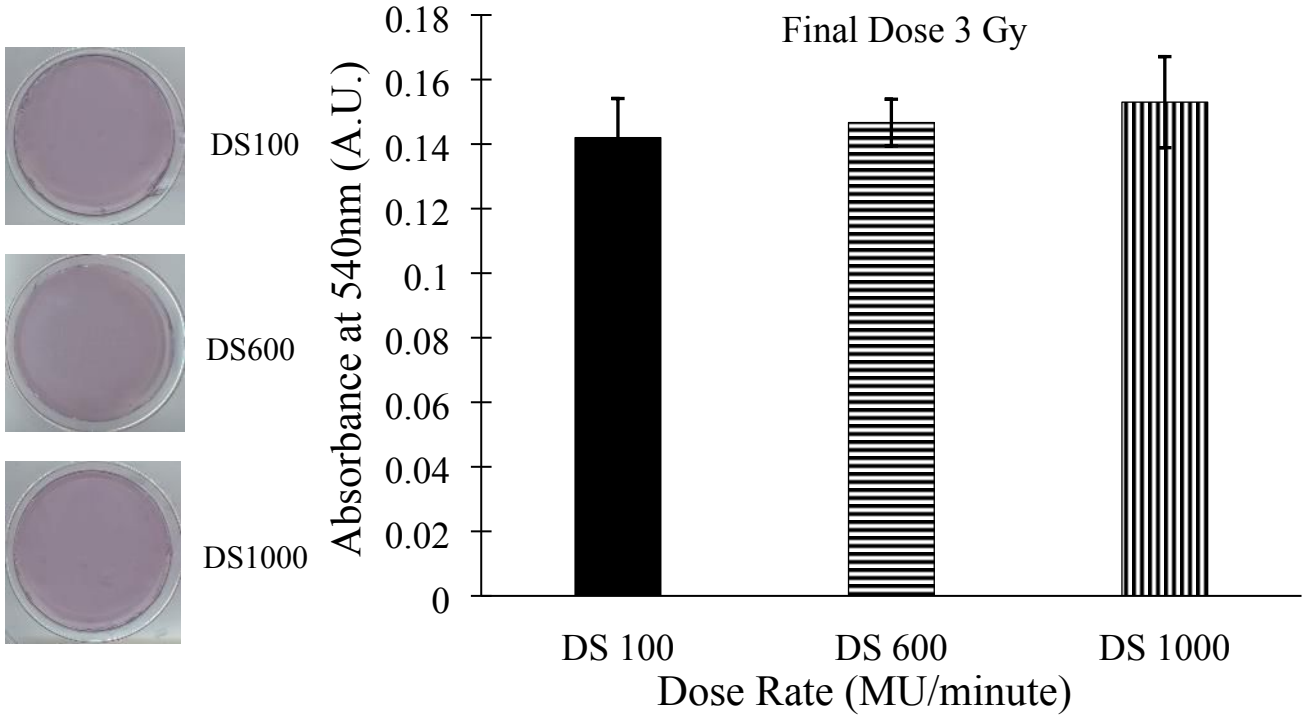

Figure 7. Absorbance at 540nm as a function of dose rate. Three different dose rates - 100, 600 and 1000 Monitor Units/minute - were employed in the study. No significant differences in absorbance or the observed color were observed, which indicates dose rate independence of the gel detection system. One-way ANOVA with $\alpha = 0.05$ was performed and no statistical significance between all three groups was observed. Image Credit: Karthik Pushpavanam, Arizona State University.

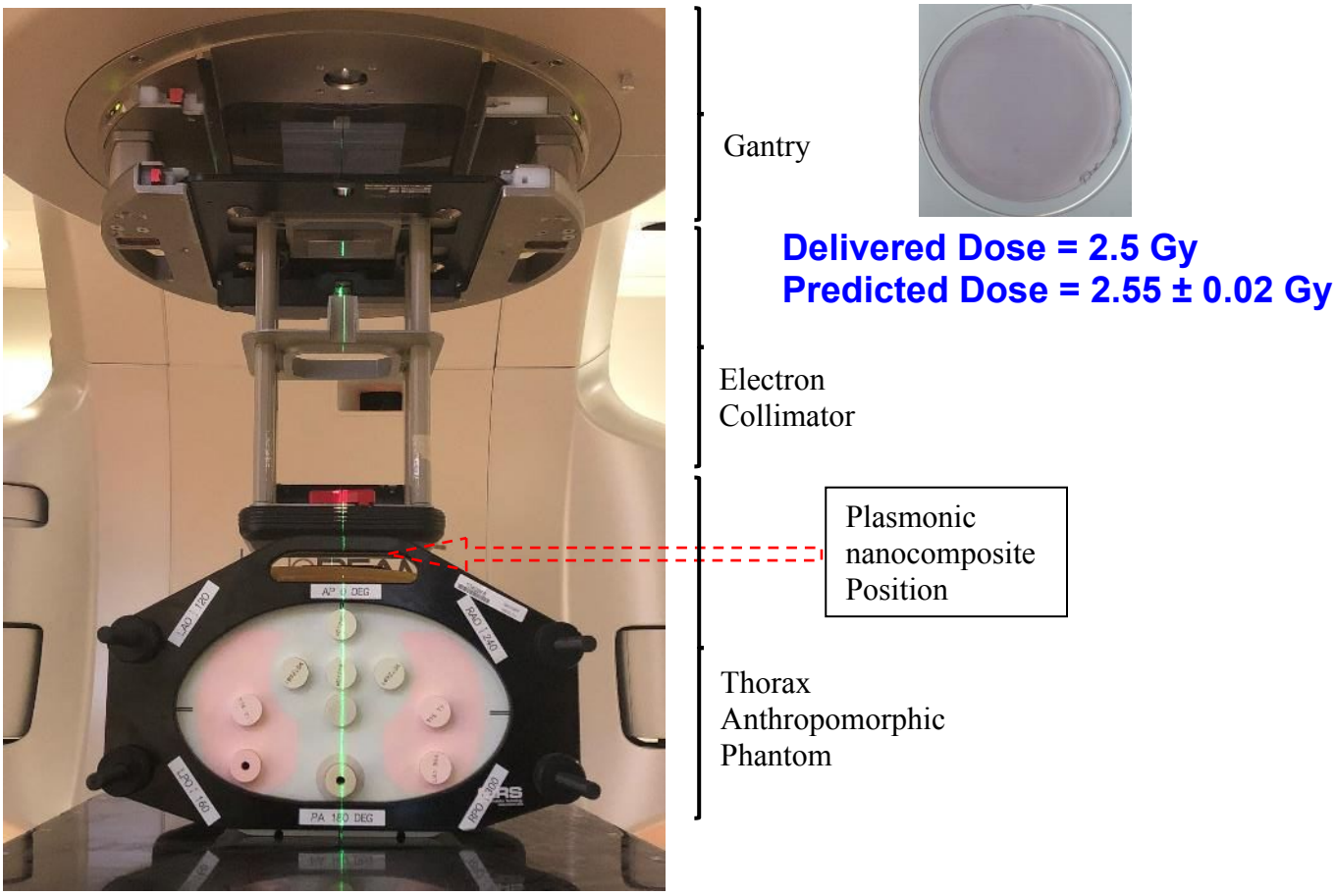

Figure 8. (Left) Setup depicting the anthropomorphic thorax phantom and **(Right)** Image of the plasmonic nanocomposite after exposure to 2.5 Gy. The plasmonic nanocomposite predicts a radiation dose of 2.55 ± 0.02Gy. Image Credit: Karthik Pushpavanam, Arizona State University.

Delivered Dose (Gy)	Predicted Dose (Gy)	Error %
1.5	1.23 ± 0.21	18
2.8	2.85 ± 0.29	1.8
4.5	4.0 ± 0.24	11

Table 1. Table indicating the efficacy of the plasmonic gel nanocomposites for predicting the dose delivered. Error percentages are lower in 2-5 Gy range for which the calibration is valid, compared to the dose outside this dose range.

REFERENCES

1. Barcellos-Hoff, M. H.; Park, C.; Wright, E. G., Radiation and the microenvironment – tumorigenesis and therapy. *Nature Reviews Cancer* **2005,** *5*, 867.
2. Baskar, R.; Lee, K. A.; Yeo, R.; Yeoh, K. W., Cancer and Radiation Therapy: Current Advances and Future Directions. In *Int J Med Sci*, 2012; Vol. 9, pp 193-199.
3. Kry, S. F.; Smith, S. A.; Weathers, R.; Stovall, M., Skin dose during radiotherapy: a summary and general estimation technique. *Journal of Applied Clinical Medical Physics* **2012,** *13* (3), 20-34.
4. Hall, S.; Rudrawar, S.; Zunk, M.; Bernaitis, N.; Arora, D.; McDermott, C. M.; Anoopkumar-Dukie, S., Protection against Radiotherapy-Induced Toxicity. *Antioxidants* **2016,** *5* (3), 22.
5. Allen, C.; Borak, T. B.; Tsujii, H.; Nickoloff, J. A., Heavy Charged Particle Radiobiology: Using Enhanced Biological Effectiveness and Improved Beam Focusing to Advance Cancer Therapy. *Mutation research* **2011,** *711* (1-2), 150-157.
6. Günhan, B.; Kemikler, G.; Koca, A., Determination of surface dose and the effect of bolus to surface dose in electron beams. *Medical Dosimetry* **2003,** *28* (3), 193-198.
7. Kainz, K. K.; Hogstrom, K. R.; Antolak, J. A.; Almond, P. R.; Bloch, C. D.; Chiu, C.; Fomytskyi, M.; Raischel, F.; Downer, M.; Tajima, T., Dose properties of a laser accelerated electron beam and prospects for clinical application. **2004,** *31* (7), 2053-2067.
8. Safigholi, H.; Song, W. Y.; Meigooni, A. S., Optimum radiation source for radiation therapy of skin cancer. *J Appl Clin Med Phys* **2015,** *16* (5), 219-227.
9. Abu-Gheida, I.; Reddy, C. A.; Kotecha, R.; Weller, M. A.; Shah, C.; Kupelian, P. A.; Mian, O.; Ciezki, J. P.; Stephans, K. L.; Tendulkar, R. D., Ten-Year Outcomes of Moderately Hypofractionated (70 Gy in 28 fractions) Intensity Modulated Radiation Therapy for Localized Prostate Cancer. *Int J Radiat Oncol Biol Phys* **2019,** *104* (2), 325-333.
10. Patel, N.; Faria, S.; Cury, F.; David, M.; Duclos, M.; Shenouda, G.; Ruo, R.; Souhami, L., Hypofractionated Radiation Therapy (66 Gy in 22 Fractions at 3 Gy per Fraction) for Favorable-Risk Prostate Cancer: Long-term Outcomes. *International Journal of Radiation Oncology • Biology • Physics* **2013,** *86* (3), 534-539.
11. Jafari, S. M.; Jordan, T. J.; Distefano, G.; Bradley, D. A.; Spyrou, N. M.; Nisbet, A.; Clark, C. H., Feasibility of using glass-bead thermoluminescent dosimeters for radiotherapy treatment plan verification. *The British journal of radiology* **2015,** *88* (1055), 20140804-20140804.
12. Saini, A. S.; Zhu, T. C., Dose rate and SDD dependence of commercially available diode detectors. **2004,** *31* (4), 914-924.
13. Sipilä, P.; Ojala, J.; Kaijaluoto, S.; Jokelainen, I.; Kosunen, A., Gafchromic EBT3 film dosimetry in electron beams — energy dependence and improved film read-out. **2016,** *17* (1), 360-373.
14. Tanooka, M.; Doi, H.; Miura, H.; Inoue, H.; Niwa, Y.; Takada, Y.; Fujiwara, M.; Sakai, T.; Sakamoto, K.; Kamikonya, N.; Hirota, S., Three-dimensional radiochromic film dosimetry for

volumetric modulated arc therapy using a spiral water phantom. *Journal of Radiation Research* **2013,** *54* (6), 1153-1159.
15. Pushpavanam, K.; Narayanan, E.; Rege, K., Molecular and Nanoscale Sensors for Detecting Ionizing Radiation in Radiotherapy. *ChemNanoMat* **2016,** *2* (5), 385-395.
16. Christensen, A. N.; Rydhög, J. S.; Søndergaard, R. V.; Andresen, T. L.; Holm, S.; Munck af Rosenschöld, P.; Conradsen, K.; Jølck, R. I., Injectable silver nanosensors: in vivo dosimetry for external beam radiotherapy using positron emission tomography. *Nanoscale* **2016,** *8* (21), 11002-11011.
17. Zeininger, L.; He, M.; Hobson, S. T.; Swager, T. M., Resistive and Capacitive γ-Ray Dosimeters Based On Triggered Depolymerization in Carbon Nanotube Composites. *ACS Sensors* **2018,** *3* (5), 976-983.
18. Liu, C.; Li, Z.; Hajagos, T. J.; Kishpaugh, D.; Chen, D. Y.; Pei, Q., Transparent Ultra-High-Loading Quantum Dot/Polymer Nanocomposite Monolith for Gamma Scintillation. *ACS Nano* **2017,** *11* (6), 6422-6430.
19. Mahan, M. M.; Doiron, A. L., Gold Nanoparticles as X-Ray, CT, and Multimodal Imaging Contrast Agents: Formulation, Targeting, and Methodology %J Journal of Nanomaterials. **2018,** *2018*, 15.
20. Chandran, P. R.; Thomas, R. T., Chapter 14 - Gold Nanoparticles in Cancer Drug Delivery. In *Nanotechnology Applications for Tissue Engineering*, Thomas, S.; Grohens, Y.; Ninan, N., Eds. William Andrew Publishing: Oxford, 2015; pp 221-237.
21. Huang, H.-C.; Barua, S.; Sharma, G.; Dey, S.; Rege, K., *Inorganic Nanoparticles for Cancer Imaging and Therapy*. 2011; Vol. 155, p 344-57.
22. Daniela, C.; Andreea, C.; Rebecca, P.; Alexandru Mihai, G., Biomedical Applications of Gold Nanoparticles. *Current Topics in Medicinal Chemistry* **2015,** *15* (16), 1605-1613.
23. Pushpavanam, K.; Narayanan, E.; Chang, J.; Sapareto, S.; Rege, K., A Colorimetric Plasmonic Nanosensor for Dosimetry of Therapeutic Levels of Ionizing Radiation. *ACS Nano* **2015,** *9* (12), 11540-11550.
24. Walker, C. R.; Pushpavanam, K.; Nair, D. G.; Potta, T.; Sutiyoso, C.; Kodibagkar, V. D.; Sapareto, S.; Chang, J.; Rege, K., Generation of Polypeptide-Templated Gold Nanoparticles using Ionizing Radiation. *Langmuir* **2013,** *29* (32), 10166-10173.
25. Thaker, A.; Pushpavanam, K.; Bista, T.; Sapareto, S.; Rege, K.; Nannenga, B. L., Protein-facilitated gold nanoparticle formation as indicators of ionizing radiation. *Biotechnology and Bioengineering* **2019,** *116* (12), 3160-3167.
26. Inamdar, S.; Pushpavanam, K.; Lentz, J. M.; Bues, M.; Anand, A.; Rege, K., Hydrogel Nanosensors for Colorimetric Detection and Dosimetry in Proton Beam Radiotherapy. *ACS Applied Materials & Interfaces* **2018,** *10* (4), 3274-3281.
27. Pushpavanam, K.; Inamdar, S.; Chang, J.; Bista, T.; Sapareto, S.; Rege, K., Detection of Therapeutic Levels of Ionizing Radiation Using Plasmonic Nanosensor Gels. *Advanced Functional Materials* **2017,** *27* (21), 1606724.
28. Pushpavanam, K.; Inamdar, S.; Dutta, S.; Bista, T.; Sokolowski, T.; Boshoven, E.; Sapareto, S.; Rege, K., Determination of topographical radiation dose profiles using gel nanosensors. *Sci Adv* **2019,** *5* (11), eaaw8704.
29. Downey, N., Extraction of DNA from Agarose Gels. In *E. coli Plasmid Vectors: Methods and Applications*, Casali, N.; Preston, A., Eds. Humana Press: Totowa, NJ, 2003; pp 137-139.

30. Thompson, L.; Dias, H. G.; Campos, T. P. R., Dosimetry in brain tumor phantom at 15 MV 3D conformal radiation therapy. *Radiat Oncol* **2013,** *8*, 168-168.
31. Piotrowski, T.; Milecki, P.; Skórska, M.; Fundowicz, D., Total skin electron irradiation techniques: a review. *Advances in Dermatology and Allergology/Postępy Dermatologii I Alergologii* **2013,** *30* (1), 50-55.
32. Licona, I.; Figueroa-Medina, E.; Gamboa-deBuen, I., Dose distributions and percentage depth dose measurements for a total skin electron therapy. *Radiation Measurements* **2017,** *106*, 365-372.
33. Coeytaux, K.; Bey, E.; Christensen, D.; Glassman, E. S.; Murdock, B.; Doucet, C., Reported Radiation Overexposure Accidents Worldwide, 1980-2013: A Systematic Review. *PLOS ONE* **2015,** *10* (3), e0118709.
34. Zeng, J.; Ma, Y.; Jeong, U.; Xia, Y., AuI: an alternative and potentially better precursor than AuIII for the synthesis of Au nanostructures. *Journal of Materials Chemistry* **2010,** *20* (12), 2290-2301.
35. Pimblott, S. M.; LaVerne, J. A., Effect of Electron Energy on the Radiation Chemistry of Liquid Water. *Radiation Research* **1998,** *150* (2), 159-169.
36. Nowicka, A. M.; Hasse, U.; Hermes, M.; Scholz, F., Hydroxyl Radicals Attack Metallic Gold. **2010,** *49* (6), 1061-1063.
37. Anandhakumar, S.; Rajaram, R.; Mathiyarasu, J., Unusual seedless approach to gold nanoparticle synthesis: application to selective rapid naked eye detection of mercury(ii). *Analyst* **2014,** *139* (13), 3356-3359.
38. Zarrintaj, P.; Manouchehri, S.; Ahmadi, Z.; Saeb, M. R.; Urbanska, A. M.; Kaplan, D. L.; Mozafari, M., Agarose-based biomaterials for tissue engineering. *Carbohydrate Polymers* **2018,** *187*, 66-84.
39. Yeh, Y.-C.; Creran, B.; Rotello, V. M., Gold nanoparticles: preparation, properties, and applications in bionanotechnology. *Nanoscale* **2012,** *4* (6), 1871-1880.
40. Mata, J.; Varade, D.; Bahadur, P., Aggregation behavior of quaternary salt based cationic surfactants. *Thermochimica Acta* **2005,** *428* (1), 147-155.
41. Pérez-Juste, J.; Liz-Marzán, L. M.; Carnie, S.; Chan, D. Y. C.; Mulvaney, P., Electric-Field-Directed Growth of Gold Nanorods in Aqueous Surfactant Solutions. **2004,** *14* (6), 571-579.
42. Akar, B.; Pushpavanam, K.; Narayanan, E.; Rege, K.; Heys, J. J., Mechanistic investigation of radiolysis-induced gold nanoparticle formation for radiation dose prediction. *Biomedical Physics & Engineering Express* **2018,** *4* (6), 065011.
43. Sharma, V. K.; Mitra, S.; Sakai, V. G.; Mukhopadhyay, R., Dynamical Features in Cationic Micelles of Varied Chain Length. *The Journal of Physical Chemistry B* **2012,** *116* (30), 9007-9015.
44. Safigholi, H.; Song, W. Y.; Meigooni, A. S., Optimum radiation source for radiation therapy of skin cancer. **2015,** *16* (5), 219-227.
45. Engel, S.; Fritz, E.-C.; Ravoo, B. J., New trends in the functionalization of metallic gold: from organosulfur ligands to N-heterocyclic carbenes. *Chemical Society Reviews* **2017,** *46* (8), 2057-2075.
46. Hall, E. J.; Brenner, D. J., The dose-rate effect revisited: Radiobiological considerations of importance in radiotherapy. *International Journal of Radiation Oncology*Biology*Physics* **1991,** *21* (6), 1403-1414.

47. Pushpavanam, K.; Inamdar, S.; Chang, J.; Bista, T.; Sapareto, S.; Rege, K., Detection of Therapeutic Levels of Ionizing Radiation Using Plasmonic Nanosensor Gels. **2017,** *27* (21), 1606724.

TABLE OF CONTENTS GRAPHIC